ICAS-88-4.9.3

SOME TYPES OF SCALE EFFECT IN LOW-SPEED, HIGH-LIFT FLOWS

D. S. Woodward, B. C. Hardy and P. R. Ashill
Royal Aircraft Establishment, Farnborough, Hampshire, UK

Abstract

Previous classifications of types of scale effect, especially on aerofoils at maximum lift, are reviewed and the salient features of each are explained. A new classification of five types of scale effect is then introduced, for high-lift flows, which embraces both the previous classification for aerofoils and observed scale effects on wings with slotted high-lift systems. Examples are given of each of these types from tests in RAE tunnels, and the important features of each are discussed, especially those which result in adverse scale effect.

Introduction

In 1968 Pearcey et al [1] produced a classification of types of flow that could occur on aerofoils at high subsonic speeds as the result of a shock/boundary layer interaction around mid-chord and the adverse pressure gradient towards the trailing-edge. Quite naturally, this classification was applied locally at points across the span of finite swept wings of moderate to high Aspect Ratio, and helped materially in the understanding and forecasting of scale effects, and with the development of transition-fixing techniques to simulate high Reynolds number flows [2,3]. Recently the current state of understanding of scale effect at high subsonic speeds was set out and considerably advanced in a paper by Elsenaar [4].

This paper sets out to perform a similar task for low-speed, high-lift flows. However, instead of classifying types of flow, so that the scale effect for each can be considered separately, it attempts to classify the dominant causes of scale effect on single and multi-element aerofoils and wings, particularly in relation to maximum lift.

For single-element conventional aerofoils, McCullough and Gault [5], have identified three main classes of stall pattern and Gault [6], after adding a fourth, has produced a correlation which identifies the appropriate stall pattern in terms of the aerofoil geometry and Reynolds number. Therefore, for this subset of low-speed, high-lift flows, the types of flow and the origins of the scale effect are well understood, and, in view of their fundamental importance, these are briefly reviewed in section 2. However there is no comparable classification for multi-element aerofoils and wings, nor is there any classification that takes into account significant effects arising from the three-dimensional development of the boundary layer on swept wings. In section 4 of this paper new classifications will be proposed which subsume Gault's aerofoil classification and cover both these other areas.

In the subsequent sections each of the new classes will be described and examples given, mostly taken from tests in the RAE 5m tunnel [7]. This tunnel has the capability to vary Reynolds number over a 3:1 range at constant Mach number by pressurization, and has opened the door to entirely new understandings of scale effect.

Some of the information and data given has already been published in an earlier paper [8], but where this occurs the data are augmented with more recently acquired data and studied from the viewpoint of scale effect, leaving aside the compressibility and project issues considered previously.

2 Gault's classification of single-element aerofoil stall

Gault [6] identifies four dominant stall patterns on single-element conventional aerofoils:

(a) thin-aerofoil stall,

(b) leading-edge stall,

(c) combined leading- and trailing-edge stall,

(d) trailing-edge stall,

and typical $C_L \sim \alpha$ curves for each of these are shown schematically in Fig 1. The flow patterns and boundary layer states for each of these are shown in Fig 2.

At the point A on each of these $C_L \sim \alpha$ curves the flow pattern and boundary layer states are similar; between A and C the flow develops differently in each case.

The flow at point A consists of a laminar boundary layer from the stagnation point to the peak suction; just beyond the peak suction the laminar boundary layer separates, and shortly afterwards (1-2% chord) transition occurs in the separated layer. The resulting turbulent flow re-attaches almost immediately to form a so-called 'short bubble', with a conventional attached turbulent boundary layer downstream to the trailing-edge. It is useful to think of this boundary layer flow as made up of these three distinct parts when we come to discuss scale effect on maximum lift coefficient ($C_{L_{max}}$):

(a) the laminar layer - which can be calculated by the method of Thwaites [9],

(b) short separation bubble - which can be calculated by the method of Horton [10],

(c) the turbulent boundary layer - which can be calculated, for example, by the lag-entrainment method [11], using as a starting condition the momentum thickness at the re-attachment position of the short bubble (θ_{RT}) obtained from Horton's method.

For thin aerofoil stall, at the point B, the re-attachment process of the short bubble fails and the bubble 'bursts' to form a 'long bubble' (5-15% chord long) with a re-attachment point further aft. As the incidence is increased the long bubble grows longer and gives rise to a corresponding increase in θ_{RT} at the re-attachment point and hence to the boundary layer thickness at the trailing-edge; ultimately the lift begins to decrease at point C as a result of this growing boundary layer thickness at the trailing-edge, and this usually happens when re-attachment occurs aft of 50% chord.

For leading-edge stall, $C_{L_{max}}$ coincides with the bursting of the short bubble because, in this case, the subsequent re-attachment of the long bubble is either close to the trailing-edge, or beyond in the wake. As thickness and/or Reynolds number is increased from an initial, well-defined, thin-aerofoil stall, the point B moves to a higher value of α and the resulting long bubble becomes progressively longer, and so there is little conceptual difference between these two stall patterns, even though the manifestations are rather different.

Ultimately, as thickness or Reynolds number is increased, the short bubble contracts until its bursting point is delayed to an incidence higher than that at which the resulting boundary layer begins to separate at the trailing-edge. Initially, the resulting separation may produce changes in pressure distribution over the region of the bubble which are significant enough to change its development (sometimes even provoking bursting as the separation begins) or small additional increases in Reynolds number produce large enough changes in bubble development to affect materially the aft separation. In some cases a local region of incipient separation has been reported just downstream of the short bubble re-attachment [12] and this too promotes subsequent separation near the trailing-edge. These interactive flow patterns are classified as 'combined leading- and trailing-edge stall'.

As thickness or Reynolds number is increased still further, the short bubble reaches such a stable state that its role effectively degenerates to that of a transition point, and the only separation that contributes to the determination of maximum lift is that at the trailing-edge; this is known as 'trailing-edge stall'.

Gault's correlation [6] of these four stall patterns with aerofoil geometry and Reynolds number is shown in Fig 3 and demonstrates clearly that a given aerofoil may have several different stall patterns depending on the relevant Reynolds number; there are several specific examples of this type of behaviour [5,13]. Furthermore it has been demonstrated [14] that these stall patterns can be identified on high aspect ratio finite wings up to 35° sweep. It will be seen later that the fundamental aspects of some of these stall patterns can also be seen on multi-element wings.

3 Origins of scale effect

Elsenaar [4] draws a distinction between the two different types of scale effect:

Direct - defined as the direct effect of Reynolds number scaling on the development of the viscous shear layer for a fixed ('frozen') pressure distribution.

Indirect - defined as the changes in the pressure distribution resulting from the direct Reynolds number effects.

This distinction is important because Elsenaar [4] cites several cases in which large indirect effects result from small direct effects - and further examples will appear in this paper.

For our purposes it is convenient to introduce a further subdivision of direct scale effect:

(a) changes in boundary layer characteristics due to Reynolds number scaling with a fixed transition position. This includes the variation of turbulent skin-fricton with Reynolds number, so that, unlike a laminar layer, a turbulent boundary-layer provides a pressure rise to separation that increases with Reynolds number;

(b) changes in transition position as a result of changes in Reynolds number.

It is important to bear both these sources in mind when analysing data from tests in low-speed, high-lift flows, because almost all of these are conducted without any attempt to fix transition. This stems primarily from the considerable difficulty of artificially stimulating transition upstream of its natural location in these flows, but even it it could be done, it would not generally result in a better representation of full-scale conditions, as can be achieved for tests at cruise Mach numbers.

It is worth considering, for a moment, the likely magnitude of the direct Reynolds number effects with a fixed transition position. The momentum thickness of a turbulent boundary layer responds to changes in Reynolds number typically as

$$\theta_{turb} \propto \frac{1}{(R)^{\frac{1}{5}}}$$

so that, for instance, a threefold increase in Reynolds number produces only a 20% reduction in boundary layer thickness. Since the majority of the boundary layer seen on an aerofoil (as shown in Fig 2) is turbulent, it could be argued it would be surprising if this small change gave rise to significant scale effect. However this would be to ignore the effect of the initial length of laminar boundary layer where momentum thickness

$$\theta_{lam} \propto \frac{1}{(R)^{\frac{1}{2}}} .$$

This relation results in the starting thickness (see Fig 4a) of the turbulent layer reducing by 43% for the same threefold increase in Reynolds number. The effect of a short bubble between the laminar layer and the turbulent layer may exert an even more dominant effect. McGregor [15] found, in at least one case, that the boundary layer momentum thickness at re-attachment

$$\theta_{RT} \propto \frac{1}{R} ,$$

and this relationship would naturally produce a 67% decrease in the starting thickness of the turbulent layer for the same threefold increase in Reynolds number (see Fig 4b).

However, part of this large variation of θ_{RT} with Reynolds number is due to the small forward movement of transition in the separated laminar shear layer, and the consequent shortening of the bubble. Because of this, part of the 67% variation ought logically to be ascribed to the second of the sources given above. However, it is convenient to ignore this distinction and regard a stable short bubble (ie one far away from bursting) as a fixed transition position.

It then becomes convenient to sub-divide movements of transition into two further sub-categories:

(i) when transition moves forward within the separated shear layer downstream of separation and this directly affects the Reynolds number and/or incidence at which bursting takes place, ie thin aerofoil and leading-edge stalls. This effect is always strongly favourable and reduces the boundary layer thickness towards the trailing-edge;

(ii) when transition moves forward of laminar separation and the bubble is eradicated. This effect usually results in an increase in boundary layer thickness towards the trailing-edge because of the increase in length of the turbulent boundary layer, and hence results in an adverse scale effect on $C_{L_{max}}$. It will be seen later how this can occur on swept wings.

4 Suggested classification of scale effect in high-lift flows

Although Elsenaar's [4] simple classification into direct and indirect effects is a valuable aid to understanding and description, it is rather too broad to provide an adequate description of the complex scale effects which can arise in low-speed, high-lift flows. Hence it was felt that a more detailed classification was needed in which the description of each the classes was closely related to the dominant flow feature involved. Based on the experience of six years of testing in the RAE 5m tunnel, the following five categories appear to cover all the aerofoil flows described before and all the types of flow observed in the tunnel on finite wings.

(a) Conventional scale effect - this class is typified by Gault's trailing-edge stall category; the direct effects stem entirely from sub-division (a) of the previous section; for lift coefficients below $C_{L_{max}}$ there is only a relatively weak interaction [4] between the viscous layers and the outer inviscid flow, so the indirect effects are small; beyond $C_{L_{max}}$ significant separations will be present and the indirect effects will be much larger.

(b) Bubble-dominated scale effect - this class is typified by Gault's leading-edge and thin-aerofoil stall categories; the dominant direct effects come from sub-division (b)(i) in the previous section; when the short bubble bursts the direct effects are large and there is a strong interaction [4] between the viscous layers and the outer inviscid flow; for this reason the scale effects in this class are usually large and occur over small regions of Reynolds number in which the flow changes very rapidly.

(c) Slot-flow-dominated scale effect - this is a complex source of scale effect which could be caused by direct effects (a) or (b)(ii) and occurs mainly on highly-deflected slotted trailing-edge flaps at low sweep; as will be seen later, the flow is dominated by the indirect effects.

(d) Three-dimensional transition-dominated scale effect - the direct effects that cause this class of scale effect come from sub-division (b)(ii) of the previous section; it occurs only on swept wings, and for sweeps typical of subsonic civil transport aircraft, occurs only for Reynolds numbers above about ½ of the full-scale value, which corresponds roughly to the Reynolds number range between that at the top of the 5m tunnel envelope and full scale; it thus represents an area of uncertainty that calls for considerable research.

(e) Scale effect in vortex-dominated flows - this occurs mainly on slender wings, or combat aircraft wings with strakes, or slender bodies; the controlling flow mechanisms are, as yet, not well understood, and hence, although the direct effects probably arise from sub-divisions (a) and (b)(ii), the role of the indirect effects cannot be described.

5 Conventional scale effect

As defined above, this arises entirely from changes in boundary layer thickness and skin friction characteristics with increasing Reynolds number, and assumes that the transition positions remain effectively fixed as the Reynolds number is increased. In terms of maximum lift, the important flow separation that produces the stall will usually originate from one of the following:

(i) the trailing-edge on a single-element aerofoil or wing; this is caused by the direct effect of the pressure rise from the peak suction to the trailing edge;

(ii) the flap shroud on a two-element aerofoil or wing (ie the wing and flap parts of Fig 5); this may be caused directly by the pressure rise between the peak suction and the shroud trailing-edge as for (i), or may be influenced by the indirect effect of a growing separation on the flap with increasing incidence, which causes the pressure at the shroud trailing-edge to become more positive as the circulation on the flap collapses;

(iii) the flap shroud on a three-element aerofoil or wing (Fig 5); this can arise from either of the sources described in (ii) above or as a result of the direct effects arising from the interaction between the slat wake and the boundary layer on the wing [16];

(iv) slat trailing-edge on a three-element aerofoil or wing (Fig 5); for many take-off configurations the slat is very highly loaded and the initial separation occurs on this element; however this may not be apparent in flow visualization because the resulting thick slat wake almost inevitably triggers off origin (iii) above, through its interaction and merging with the wing boundary layer.

The behaviour of maximum lift on a 1/13 scale model of an A300B tested in the 5m tunnel at M = 0.21 is a good example of this type of scale effect. Fig 6 shows that, for this model, the top of the lift curve is rounded, the progression of $C_{L_{max}}$ with increasing Reynolds number is smooth with a monotonically decreasing gradient, and the total increment, whilst not negligible, is relatively low $(\Delta C_{L_{max}} < 0.05)$.

6 Bubble-dominated scale effect

As set out in section 4 this embodies both 'thin-aerofoil' and 'leading-edge' stall in

two-dimensional flow and also on finite swept wings. It arises, as its name implies, from the 'bursting' of the short laminar separation bubble.

The first example of this type of scale effect comes from tests on a 0.315 scale model of a BAe Hawk in the RAE 5m tunnel at Reynolds numbers up to full scale ; the top of the $C_L \sim \alpha$ curve and the progression of $C_{L_{max}}$ with increasing R are shown in Fig 7 for the wing configuration in which the stall trips have been removed [8]. It will be seen that

(a) the stall, especially at $R = 4.1 \times 10^6$ is very sharp and similar to the leading-edge stall pattern shown in Fig 1;

(b) the total increment over the Reynolds number range, $\Delta C_{L_{max}} \triangleq 0.18$, is much larger than for the A300B model.

If these $\Delta C_{L_{max}}$ figures were based on exposed area, the difference between Hawk and A300B would be even more marked due to the large area increase of the A300B high-lift system compared with that of the Hawk.

In addition, it is known, from early flight testing before the current stall trips were developed, that the stall then was very sudden, usually involving a wing drop, and that in-flight oil flow visualization showed a laminar bubble existing near the leading-edge [17].

The second example is of a much more extreme nature and occurs on a half-model with a simple, tapered, untwisted wing (Model 477), fitted with a 12½% chord slat and a single-slotted flap at 20°. Previous work [8] examining the movement of the optimum slat position with Reynolds number, had concentrated on just three widely-spaced Reynolds numbers. The progression of $C_{L_{max}}$ with increasing Reynolds number had appeared to be rapid but just as smooth as those already shown for A300B and Hawk. However, recent work at much more closely spaced Reynolds numbers shows that $C_{L_{max}}$ varies extremely rapidly over part of the Reynolds number range as shown in Fig 8.

Early flow visualization work in the 13ft × 9ft atmospheric tunnel at RAE Bedford had shown that the initial stall took place as a complete separation of the flow over the outboard 30% of the slat span. This had been 'cured' by adding roughness to this portion of the slat, but the results showed a remarkable sensitivity to roughness position and spanwise extent (Fig 9). In Fig 10 the normal forces on the wing and slat (obtained by integration of the pressure measurements on a section at 84% span) are plotted against incidence. It will be seen that, with no roughness, loss of lift occurs simultaneously on both slat and wing, whereas, with roughness on, the initial loss of lift occurs on the wing, and the slat lift continues to rise for a small additional increment in α .

From these facts, it is reasonable to deduce that, at Reynolds numbers below about $3.2 \rightarrow 3.5 \times 10^6$ (Fig 8), $C_{L_{max}}$ is determined by bubble bursting on the slat, whereas, at Reynolds numbers above this, the stall pattern changes to one where the initial separation occurs near the trailing edge of the main wing (ie the flap shroud) and hence the subsequent scale effect is of the conventional type. This set of data underlines the importance of pressurized wind tunnels because of their ability to produce wide variations of Reynolds number at constant Mach number. Model 477 was designed before the RAE 5m tunnel was available and was intended to produce, in an atmospheric 13ft × 9ft tunnel, the maximum possible Reynolds number on a tapered planform with:

(a) a high enough Aspect Ratio to ensure some portion of the span in which there existed a genuine sheared wing flow free from the effects of the root and tip;

(b) a change in sweep from leading- to trailing-edge which was representative of a typical transport aircraft wing.

Despite this design aim, this particular slat configuration has displayed a remarkable sensitivity to scale effect, and this was almost entirely unsuspected until the tests in the 5m tunnel. A large amount of the testing in the atmospheric 13ft × 9ft tunnel is now of limited use because of this exaggerated scale effect.

7 Slot-flow dominated scale effect

A typical example of this type of scale effect is shown in Fig 11, taken from some tests done for a customer in the RAE 5m tunnel on a high Aspect Ratio, low-sweep, transport wing. At low Reynolds numbers, the flow on the highly-deflected slotted flap is attached over the whole of the pre-stall incidence range, but the lift curve has a well-rounded top; at the intermediate Reynolds number, the flow on the flap is separated at low incidence, but then attaches, as incidence is increased, giving a sharp increase in lift and a characteristic nonlinear lift curve which ultimately reaches a higher $C_{L_{max}}$ and with a less well-rounded top to the lift curve; at high Reynolds number, the flap flow is separated over the entire incidence range, and the $C_{L_{max}}$ is significantly lower than it was at lower Reynolds numbers.

Exactly the same type of behaviour is displayed by the flow over a highly-deflected slotted flap on a quasi-two-dimensional end plate model at constant Reynolds number, but, this time, with a varying flap gap [18] (Fig 12). At small gaps, there is a significant interference between the main wing, plus its wake, and the flap, which leads to a reduction in the peak suction on the flap, and hence to an attached flow. As incidence is increased, the thickness of the wing wake increases too, and this is amplified in the flow over the flap by the adverse pressure gradient and wake/boundary layer interaction. The displacement effect of this thick viscous layer leads to a large lift loss relative to the inviscid level, which increases with increasing incidence, and hence to the rounded top to the lift curve shown. At intermediate gaps, the interference between the main wing plus wake and the flap at low incidence, is not large enough to depress the peak suction sufficiently to allow an attached flow. However, as incidence increases, the thickness of the wing wake increases, and, at some point, the resulting interference is sufficient to permit an attached flow

(Fig 13). The resulting viscous layer over the flap is then thinner than at the smaller gaps, and hence the lift is greater at a given incidence, as shown. At the largest gaps, the interference never becomes sufficiently large to cause the flap flow to attach, and hence the lift at all incidences is lower than at the smaller gaps and a lower $C_{L_{max}}$ is also achieved.

With increasing Reynolds number, the boundary layers and wakes reduce in thickness and hence the resulting behaviour is strikingly similar to that achieved by increasing the flap gap at constant Reynolds number.

This particular case is interesting, because it demonstrates a situation where the favourable direct Reynolds number effect is overridden by the unfavourable indirect effect; more usually, as in the cases cited by Elsenaar [4], the indirect effects are also favourable.

Clearly the identification of this type of scale effect is of major importance; a flap configuration which performs well in the 5m tunnel at, say, ¼-full scale, could turn out, at full scale, to have a performance that fell well short of that predicted due to this type of scale effect.

8 Three-dimensional transition-dominated scale effect

8.1 Introduction

Referring back to Fig 5, on aerofoils, transition takes place in the separated layer after laminar separation, and, because of the strong accelerating pressure gradients over the nose of the aerofoil, there is no natural mechanism by which transition can be brought forward of the peak suction. Indeed it is doubtful if it can even be brought forward of laminar separation, because of the short distance between the peak suction and laminar separation.

However, if we now consider the flow over an infinite yawed wing with the same pressure distribution normal to the leading-edge, there are two three-dimensional mechanisms which may permit transition to occur before the peak suction, and a two-dimensional mechanism which may work to counter the effect of this happening; these are set out below.

8.1.1 Transition due to crossflow instability

For the flow over a swept wing, the streamlines just above the boundary layer are curved in plan view by an amount depending upon the wing sweep and the pressure distribution. At each position along the streamline, the net pressure force is exactly balanced by the centrifugal force due to the velocity and the curvature.

Within the boundary layer the velocity is reduced and the streamline curvature has to change to restore the balance, with the result that a cross-flow develops. Numerous experiments [19,20] have established that this crossflow can become unstable and lead to transition, this instability being characterized by the 'crossflow Reynolds number - χ' [20], defined as

$$\chi = \frac{V_{max}\,\delta_c}{\nu} , \qquad (1)$$

where V_{max} = maximum value of the crossflow velocity within the boundary layer

δ_c = crossflow boundary layer thickness

$$= \int_0^\infty \left(\frac{V}{V_{max}}\right) dz$$

ν = kinematic viscosity.

The value of χ leading to transition has been found [21] to be in the range

$$100 < \chi < 140. \qquad (2)$$

8.1.2 Attachment line transition (ALT)

The exact solution of the Navier-Stokes equations for the flow at a two-dimensional stagnation point [22] shows that there exists a non-zero boundary layer thickness at the stagnation point, that this is constant along the surface away from the stagnation point, and that the thickness depends upon the velocity gradient away from the stagnation point, such that

$$\delta \propto \sqrt{\frac{\nu}{a}} , \qquad (3)$$

where δ = boundary layer thickness, defined as the point where the velocity decrement is 1%

ν = kinematic viscosity

a = velocity-gradient away from the stagnation point on the surface.

If we now consider the situation near the attachment line on an infinite swept wing, and invoke (a) the independence principle and (b) simple sweep theory, we find that the boundary layer characteristics that develop under the influence of the outer flow component normal to the leading-edge are identical to the stagnation point flow, but that a cross-flow develops under the influence of the outer flow component parallel to the leading-edge. The resulting three-dimensional boundary layer will have a constant thickness spanwise along the attachment line.

Fig 14 is a diagram of this flow abstracted from the work of Poll [23]. It has been known for quite a long time that, when the sweep or Reynolds number is high enough, the cross-flow along the attachment line becomes unstable and disturbances of sufficient size are propagated along the attachment line leading to transition to turbulence at the attachment line itself [24,25,26,27]. The resulting turbulent layer then spreads out spanwise and chordwise, so that, if the initial disturbance is near the root, the whole wing may become immersed in a turbulent boundary layer and there is no region downstream of the attachment line which has a laminar boundary layer. The arguments given in section 3 clearly indicate that this type of behaviour is likely to cause an adverse scale effect on the boundary layer thickness near the trailing-edge.

Poll [23,24,28] investigated this process in detail and confirmed earlier deductions that attachment line transition could be characterized by a Reynolds number formed from

(a) the velocity parallel to the leading edge, $U \sin \phi$,

and (b) a characteristic length $\eta (= \sqrt{\nu/a})$ which is proportional to the thickness of the boundary layer in the stagnation point flow.

Hence, this Reynolds number $\bar{R}$, is defined as

$$\bar{R} = \frac{U \sin \phi}{\nu} \sqrt{\frac{\nu}{a}} \quad , \tag{4}$$

where U = freestream velocity

ϕ = sweep of the leading-edge, or attachment line

a = velocity gradient normal to, and away from, the attachment line, as before.

This can be manipulated to give, for an infinite swept wing,

$$\bar{R} = \sin \phi \sqrt{\frac{R}{a}} \quad , \tag{5}$$

where R = Reynolds number, based on a streamwise reference length and velocity.

Poll found that critical values of $\bar{R}$ for transition varied to some extent with disturbance (ie roughness) level, but that, for large disturbances, such as might arise from the fuselage boundary layer, transition occurred for

$$\bar{R} > 300 \quad .$$

From equation (5) it can be seen that critical values of $\bar{R}$ can be achieved in one of three ways:

(a) high Reynolds number;

(b) high sweep;

(c) low velocity gradient - which implies low curvature.

It is the last of these which is the dominant one in producing attachment line transition on typical advanced swept wings with deployed high-lift devices, because the curvature, at typical positions of the attachment lines on the wing and the slat, is low compared with that at the position of the attachment line under cruise conditions.

8.1.3 Re-laminarisation

Launder and Jones [29] have found that, if a turbulent boundary layer is subjected to a strongly favourable pressure gradient, it is possible for the turbulence to decay and for a laminar layer to be re-established. They characterize this process in two dimensions by the parameter

$$K = \frac{\nu}{U^2} \frac{du}{dx} \tag{6}$$

and find that re-laminarisation is a possibility for

$$K > 3 \times 10^{-6} \tag{7}$$

and is highly probable if

$$K > 5 \times 10^{-6} \quad . \tag{8}$$

To use this in three-dimensional flow, Beasley [30] has suggested that K should be applied along a streamline, and that suggestion has been followed in the analysis for this paper.

8.2 Preliminary assessments of three-dimensional transition-dominated scale effect

Three-dimensional transition-dominated scale effect was first investigated at RAE around 1975 as part of an investigation into leading-edge high-lift systems having a lower drag than that of slats. Attention was directed towards a flexible Krueger leading-edge, similar to that on a Boeing 747, but which was unslotted; the shape of the flexible skin in the extended position was specially designed to give a short 'roof-top' in the pressure distribution at around maximum lift. By performing two-dimensional boundary layer calculations on the inviscid pressure distributions, it was possible to obtain approximate estimates of $C_{L_{max}}$, and C_L/C_D at take-off C_L, and their variation with Reynolds number. These showed that this device, when compared with others on the same basis, had

(a) higher $C_{L_{max}}$,

(b) much better values of sectional C_L/C_D at take-off C_L,

(c) scale effect was strongly favourable, especially on C_L/C_D.

Further investigation showed that these advantages were primarily due to the much longer predicted run of laminar boundary layer on this device than on any of the others - hence a further investigation was mounted on similar lines to determine:

(A) under what conditions this long length of laminar flow might disappear,

(B) what was the sensitivity of the results to the length of laminar flow.

The laminar boundary layer was recalculated using Beasley's [30] method which contains all the transition criteria set out in section 8.1; these calculations showed, for this device, that:

(i) attachment line transition (ALT) was most likely to occur for Reynolds numbers above about ½-full scale for typical transport wings;

(ii) transition due to cross-flow instability was unlikely to occur until a Reynolds number about

twice that for the onset of attachment line transition. This is because, even for this flexible Krueger, the laminar run is still not really long enough for much cross-flow to develop;

(iii) re-laminarisation was a possibility over only small ranges of Reynolds number near the onset of attachment line transition (ALT).

Subsequent calculations for other, more relevant, leading-edge high-lift devices, have shown that these three conclusions apply broadly to most high-lift situations - and hence that ALT is the dominant source of this type of scale effect.

To test the sensitivity of $C_{L_{max}}$ to the onset of ALT, the boundary layer was re-calculated with a turbulent boundary layer from the stagnation point - and revealed a possible loss in $C_{L_{max}}$ of around 10%. The results of this investigation are summarised in Fig 15.

8.3 Experimental programme

The results of the investigation in section 8.2 were sufficiently disturbing to warrant an experimental investigation on a more representative leading-edge high-lift system in the 5m tunnel. A detailed investigation [31] was launched using a subsonic strike fighter research model (Model 495) with hot film gauges positioned near the trailing-edge of the slat heel at three stations across the span, in order to detect the onset of ALT on the slat. In this case it would be expected that the thicker slat wake resulting from ALT, would promote wake/boundary layer interaction over the wing, and produce a reduction in $C_{L_{max}}$. During the tests at closely spaced Reynolds numbers, the following measurements were taken:

(a) records of the outputs from the hot film gauges;

(b) overall forces up to, and beyond, the stall;

(c) pressure distributions at three spanwise positions.

Some aspects of the results of this experiment were rather difficult to understand, and hence a similarly detailed investigation was carried out on Model 477 with a plain leading-edge [32]. This configuration has a much simpler attachment line, uninterrupted by slat brackets. Analysis of these two experiments is still continuing (although the Model 495 one is now near to completion) and the flows revealed are, not surprisingly, complex, so that only a selection of the most significant results are presented in the next section.

8.4 Results of experimental programme

The hot film gauges gave clear indications of the state of the attachment line boundary layer. Fig 16 shows some typical oscilloscope traces from the Model 477 attachment line with increasing Reynolds number at a constant incidence about 5° below maximum lift.

Turbulent spots are first seen at the root and then progressively at the further outboard stations; but the frequency of occurrence of the spots increases much more rapidly with Reynolds number at the outboard stations, so that the onset of complete turbulence occurs first near the tip and moves inboard.

Fig 17 shows the variation of the intermittency factor, inferred from these and other traces, with Reynolds number at various stations across the span. Qualitatively, some variation of this type would be expected, since $\bar{R}$ varies across the span, even at constant incidence, due to the spanwise variation of R/a (equation 5),

(a) R increases inboard (ie increasing $\bar{R}$) because of the larger chord arising from the tapered planform.

(b) a decreases outboard (ie increasing $\bar{R}$) because of the higher effective incidence (or local lift coefficient) there, arising from the spanwise variation of induced downwash from the trailing vorticity. At higher effective incidences the attachment line is further round the profile on the lower surface (see Fig 5) and here the curvature is lower, effectively reducing the velocity gradient "a".

For the fixed incidence relevant to Figs 16 and 17, it would be reasonable to assume that the variation of "a" at a given spanwise position with changing Reynolds number is small. This would imply that $\bar{R} \propto \sqrt{R}$ at each spanwise position and hence that the attachment-line transition front would move progressively along the leading-edge, giving lines on Fig 17 which were more-or-less parallel, rather than the diverging pattern from $R = 1.0 \times 10^6$ that is shown.

The net effect of the two conflicting factors (a) and (b) above, as incidence is varied, may be seen from Fig 18 which shows, for the slat heel of Model 495, the Reynolds number at which ALT would be expected to occur at each of the spanwise stations, assuming ALT occurs when $\bar{R} = 300$. The figure suggests, for instance, that if incidence is increased above 15°, at $R = 10 \times 10^6$, ALT will occur first outboard and progress inboard; however, for $\alpha > 29°$, the attachment line at the outboard end of the slat may revert to a laminar, or transitional, state.

Figs 19 to 21 show the observed character of the attachment line boundary layer on the slat heel of Model 495 (obtained from the hot-film gauges) as a function of incidence for various Reynolds numbers at each of the three spanwise stations. Also shown on these Figures are curves identifying the combinations of incidence and Reynolds number which yield $\bar{R} = 300$, ie they are replots of the data on Fig 18. From these Figures it can be seen that, at the outboard station (3)(Fig 19), the onset of a turbulent attachment line is roughly correlated with the line for $\bar{R} = 300$; however, at the inboard stations (1) and (2) (Figs 21 and 20), a fully turbulent attachment line does not occur until $\bar{R}$ values much higher than this. This behaviour suggests that the attachment line near the root is not experiencing 'gross contamination' (as Poll calls it) from the turbulent boundary layer on the fuselage despite the fact that, on this model, the slat is carried through the fuselage side.

Even more surprising, is that analysis of the pressure distributions at the outboard station (3) suggests strongly that the laminar separation bubble is suppressed for all values of $R \geq 7.5 \times 10^6$. According to the hot-film gauge records, the attachment line at this Reynolds number is still only transitional. However, the pressure distribution along the 'aerodynamic upper surface' shown in Fig 22, demonstrates a fairly long run of almost zero pressure gradient before the acceleration up to the peak suction is reached. It seems possible that this length of zero pressure gradient is long enough to allow the transitional attachment line flow to mature into a fully turbulent boundary layer, and hence suppress the laminar bubble.

The measured $C_{L_{max}}$ values for Model 495 (Fig 23) display the kind of variation with increasing Reynolds number that was qualitatively predicted to occur with the onset of ALT; it shows a fairly rapid rise at low Reynolds number followed by a distinct decrease (although nowhere near as large as that predicted for the flexible Krueger) occurring smoothly over a wide range of Reynolds numbers due to the fairly slow spread of ALT across the span. It will be seen that the first 'downturn' in the $C_{L_{max}}$ curve (ie where it departs from the variation indicated at the lower Reynolds numbers) can be plausibly correlated with the Reynolds number at which the laminar bubble at the outboard station (3) first disappears - thus supporting the description of the flow development given above. The figure clearly indicates the error that would have occurred in the prediction of $C_{L_{max}}$ at $R = 15 \times 10^6$ by extrapolation of data taken for $5 \times 10^6 < R < 7.5 \times 10^6$.

Finally, Fig 24 shows the variation of $C_{L_{max}}$ with Reynolds number for Model 477 fitted with the plain leading-edge. This Figure, surprisingly, shows no adverse scale effect on $C_{L_{max}}$ similar to that on Model 495, despite the clear indications of the existence of ALT given in Figs 16 and 17. Later, careful oil-flow investigations revealed that the laminar bubble still existed at all Reynolds numbers, clearly indicating the existence, and importance, of re-laminarisation for this configuration. Since the effects of ALT are effectively nullified by the re-laminarisation, it is concluded that the scale effect above about $R = 4.3 \times 10^6$ (where ALT sets in) must still be attributed to 'conventional scale effect' - as indicated on Fig 24.

9 Scale effect in Vortex-dominated flows

Vortex-dominated flows occur over slender wings, combat aircraft with highly-swept strakes, and slender bodies. Although significant scale effects have been observed on the out-of-plane forces on slender bodies [4,8], it has been generally assumed that the scale effect on the other two flows is small - primarily because the leading-edge radii in these cases are usually small, and hence the primary separations giving rise to the vortices, are fixed.

Several recent tests in the 5m and 8ft × 8ft tunnels at RAE would appear to confirm this - at least in respect to the overall forces and movements at zero yaw. The overall force results shown in Fig 25, taken on a large half-model of a wing/body combination with a cambered delta wing (Model 2205) in the 8ft × 8ft tunnel, are typical of this. However Fig 26, which shows spanwise pressure distributions taken at the same time, demonstrates clearly that there are significant scale effects on the size and position of the leading-edge vortex - although it is suspected that the circulation round the vortex is probably not much changed.

Since Model 2205 has a rounded leading-edge, it is possible that the three-dimensional transition effects described in section 8 contribute to these scale effects on the vortex; the analysis to date finds $\bar{R}$ values around 400 even at the lowest Reynolds number on Fig 26, indicating strongly that ALT is present at all the test Reynolds numbers; analysis of the probability of re-laminarisation is continuing. However, this particularly graphic demonstration of scale effect on vortex size and position does not stand alone - it is supported by evidence from other older tests [33,34,35,36] and by data taken on other models in the RAE 5m tunnel.

The results have significant implications for tests under yawed conditions. It is known that quite small angles of sideslip can produce large changes in pressure distribution on regions of a slender wing beneath leading-edge vortices [37] and can cause vortex breakdown to occur further upstream on the leading wing [37]. Also, complex forebody/leading-edge flows can affect the flow over the fin region [38] and the position of fins can influence vortex breakdown position under combined angle of attack and side-slip conditions [39]. Because of this evidence, and the evidence above of scale effect on size and location of vortices, it seems highly probable that significant scale effects will be observed on modern combat aircraft under yawed conditions, and this will be particularly significant for the design of Flight Control Systems when the basic aircraft configuration is designed to have marginal, or unstable, characteristics.

10 Conclusions

A set of five general, and very different, classifications of scale effect in low-speed, high-lift flows has been proposed and examples have been given for each from tests in RAE tunnels. The behaviour of each has been described within the conceptual framework recently set up by Elsenaar [4] for describing scale effects. Thus the examples demonstrate that in this flow regime, as at high subsonic speeds, scale effects stem from a number of different direct sources, and the way in which each is manifest depends both on which of these sources is dominant, and on the nature of the associated indirect effects. The examples further demonstrate the variety of scale effect in low-speed flows and underline the importance of testing over a range of the highest Reynolds numbers available if a confident prediction of full-scale characteristics is desired.

11 References

1 H.H. Pearcey, J. Osborne, A.B, Haines; 'The interaction between local effects at the shock and rear separation - a source of significant scale effects in wind tunnel tests on aerofoils and wings'. Paper 11, AGARD CP 35 (1968)

2 A.B. Haines; 'Possibilities for scale effects on swept wings at high subsonic speeds'. ARA Report No.18 (1971)

3 A.B. Haines; 'Further evidence, and thoughts, on scale effect at high subsonic speeds'. Paper 43, AGARD CP 174 (1975)

4 A. Elsenaar; 'On Reynolds number effects and simulation'. Paper 20, AGARD CPP 429 (1987)

5 G.B. McCullough, D.E. Gault; 'Examples of three representative types of aerofoil section stall at low speed'. NACA TN 2502 (1951)

6 D.E. Gault; 'A correlation of low-speed airfoil section stalling characteristics with Reynolds number and airfoil geometry'. NACA TN 3963 (1957)

7 A. Spence, D.S. Woodward, M.T. Caiger, A.J. Sadler, R.W. Jeffery; 'The RAE 5-metre pressurized low-speed wind tunnel'. ICAS Paper B3-05 (1978)

8 S.P. Fiddes, D.A. Kirby, D.S. Woodward, D.H. Peckham; 'Investigations into the effects of scale and compressibility on lift and drag in the RAE 5-metre pressurized low-speed wind tunnel'. Journal Roy. Aero. Soc., March 1985

9 B. Thwaites (Ed), 'Incompressible aerodynamics'. Fluid Motion Memoirs. Clarendon Press (1960)

10 H.P. Horton; 'A semi-empirical theory for the growth and bursting of laminar separation bubbles'. ARC CP 1073 (1967)

11 J.E. Green, D.J. Weeks, J.W.F. Brooman; 'Prediction of turbulent boundary layers and wakes in compressible flow by a lag-entrainment method. ARC R&M 3791 (1972)

12 R.A. Wallis; 'Boundary layer transition at the leading-edge of thin wings and its effect on general nose separation'. Advances in Aeronautical Sciences, 3, pp 161-184, Pergamon Press (1962)

13 D.S. Woodward; 'The two-dimensional characteristics of a 12.2% thick RAE 100 aerofoil section'. ARC R&M 3648 (1971)

14 D.S. Woodward, D.E. Lean; 'The lift and stalling characteristics of a 35° swept back wing designed to have identical chordwise pressure distributions at all spanwise stations when near maximum lift'. ARC R&M 3721 (1973)

15 I. McGregor; 'Regions of localised boundary-layer separation and their role in.the nose-stalling of aerofoils'. PhD Thesis, QMC London (1954)

16 D.N. Foster, P.R. Ashill, B.R. Williams; 'The nature, development, and effect of the viscous flow round an aerofoil with high lift devices'. ARC CP 1258 (1974)

17 H. Frazer-Mitchell; 'Verbal communication'. (1980)

18 B.S.P. Finch, J.R. Wedderspoon; 'Investigation into the performance of a 40° single-slotted flap on a quasi two-dimensional endplate model'. BAe Weybridge, Aero/FM/Report 046 (1978)

19 A. Anscombe, L.N. Illingworth; 'Wind tunnel observations of boundary layer transition on a wing at various angles of sweepback'. ARC R&M 2968 (1952)

20 J.T. Stuart; 'The instability of three-dimensional boundary layers'. Section 6, Chapter 9 ('Hydrodynamic stability') in 'Laminar boundary layers' (edited by L. Rosenhead), pp 549-555, Oxford University Press (1963)

21 M.G. Hall, D.A. Treadgold; 'Difficulties in predicting boundary-layer transition on swept wings'. RAE Technical Memorandum Aero 1465 (1972)

22 H. Schlichting; 'Boundary layer theory', pp 70-75. Pergamon Press (1955)

23 D.I.A. Poll; 'Some aspects of the flow near a swept attachment line with particular reference to boundary layer transition'. Cranfield Institute of Technology, College of Aeronautics Report 7805 (1978)

24 D.I.A. Poll; 'Transition in the infinite swept attachment line boundary layer'. Aeronautical Quarterly, Vol.XXX, Pt 4, pp 607-629 (1979)

25 W.P. Fenninger; 'Laminar flow control - laminarisation'. Special course on 'Concepts for drag reduction'. AGARD Report 654 (1977)

26 N. Gregory, E.M. Love; 'Laminar flow on a swept leading-edge - final progress report'. NPL Aero Memorandum 26 (1965)

27 M. Gaster; 'On the flow along swept leading-edges'. Aeronatical Quarterly, Vol.XVIII, pp 165-184 (1967)

28 D.J. Paisley, D.I.A. Poll; 'Further studies of flow over swept back wings'. Cranfield Institute of Technology, College of Aeronautics Contractors Report NFP 4 (1983)

29 B.E. Launder, W.P. Jones; 'On the prediction of laminarisation'. ARC CP 1036 (1969)

30 J.A. Beasley; 'Calculation of the laminar boundary layer and prediction of transition on a sheared wing'. RAE Technical Report 73156 (1973)

31 B.C. Hardy, D.S. Woodward; 'An experimental investigation of attachment line transition on the slat of a low-speed, high-lift, strike-fighter model. RAE Technical Report (to be published)

32 B.C. Hardy; 'An experimental investigation of attachment line transition on the leading-edge of a 30° swept wing model fitted with a plain leading-edge and a 20° single-slotted flap. RAE Technical Report (to be published)

33 E.C. Polhamus, B.B. Gloss; 'Configuration aerodynamics'. NASA CP 2183, pp 217-234 (1980)

34 W.P. Henderson; 'Effect of using leading-edge radius and Reynolds number on the longitudinal aerodynamic characteristics of highly-swept wing-body configurations at subsonic speeds. NASA TN D-8361 (1976)

35 J.E. Lamar; 'In-flight and wind tunnel leading-edge vortex study on the F106B airplane. NASA CP 2416 (1986)

36 F.W. Dee, O.P. Nicholas; 'Flight determination of wing flow patterns and buffet boundaries for the Fairey Delta 2 aircraft at Mach numbers between 0.4 and 1.3 and comparison with wind tunnel results'. ARC R&M 3482 (1967)

37 D.H. Peckham; 'Low speed wind tunnel tests on a series of uncambered slender pointed wings with sharp edges. RAE Technical Report Aero 2613 (1958)

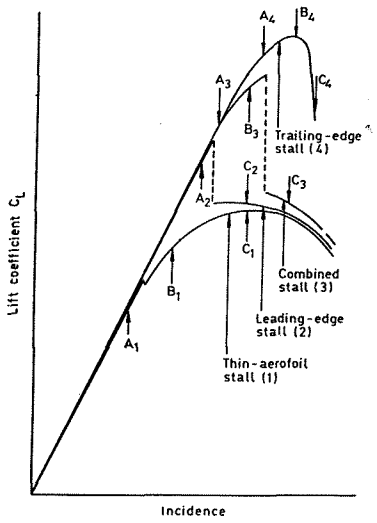

Fig 1 Typical $C_L \sim \alpha$ plots for four different aerofoil stall patterns

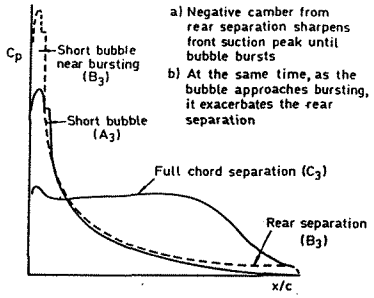

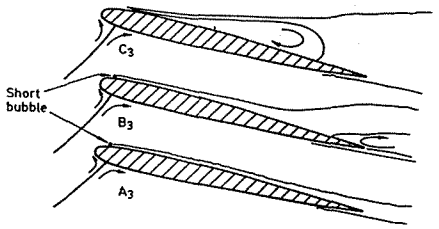

Fig 2c Pressure distributions and boundary layer states through combined stall

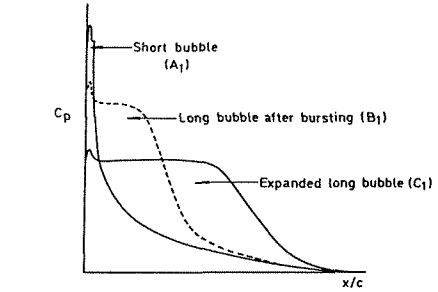

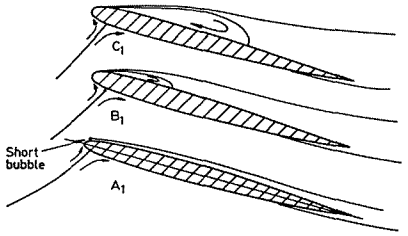

Fig 2a Pressure distributions and boundary layer states through thin-aerofoil stall

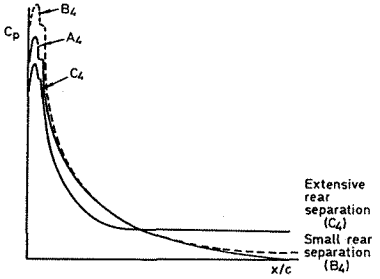

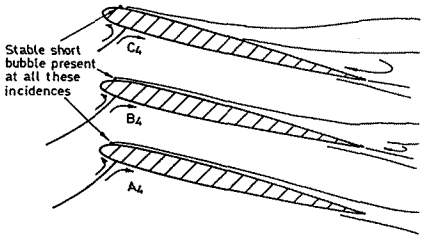

Fig 2d Pressure distributions and boundary layer states through trailing-edge stall

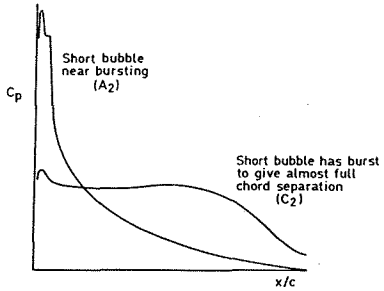

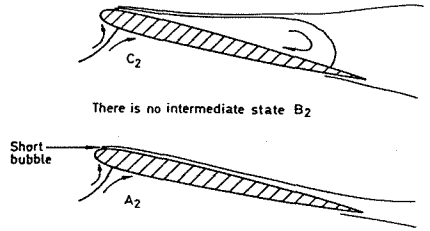

Fig 2b Pressure distributions and boundary layer states through leading-edge stall

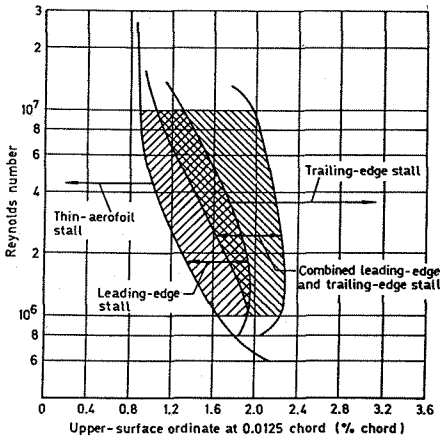

Fig 3 Correlation of aerofoil stall patterns $10^6 < R < 10^7$ (abstracted from Ref 5)

38 G.E. Erickson, W.P. Gilbert; 'Experimental investigation of forebody and wing leading-edge vortex interaction at high angles of attack'. AGARD CP 342, Paper 11 (1983)

39 D.J. Peake, M. Tobak; 'On issues concerning flow separation and vortical flows in three-dimensions'. AGARD CP 342, Paper 1 (1983)

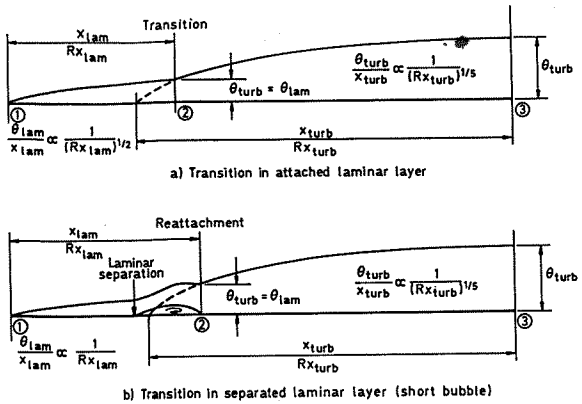

Fig 4 Origin of scale effect due to Reynolds number scaling of viscous layer thickness

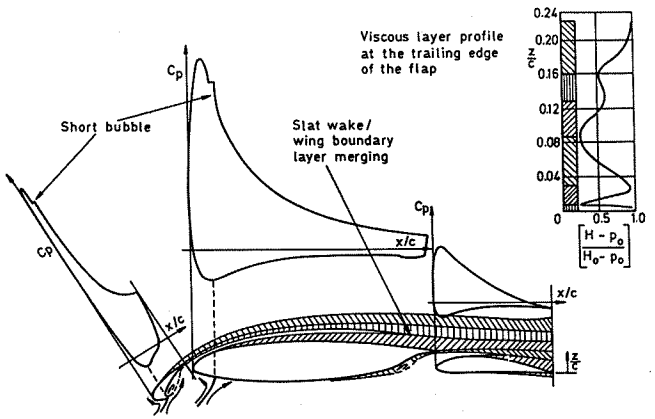

Fig 5 Pressure distributions and viscous layer states on slat/wing/flap combination

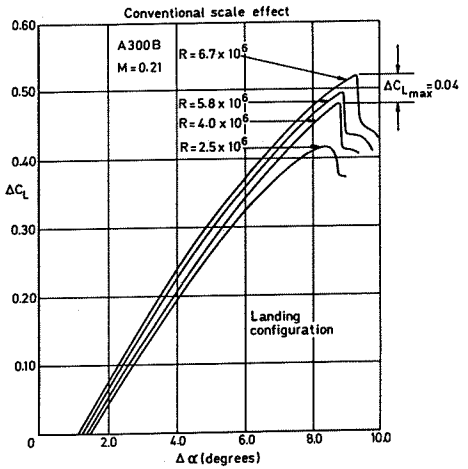

Fig 6 Variation of lift curve with Reynolds number of A300B model

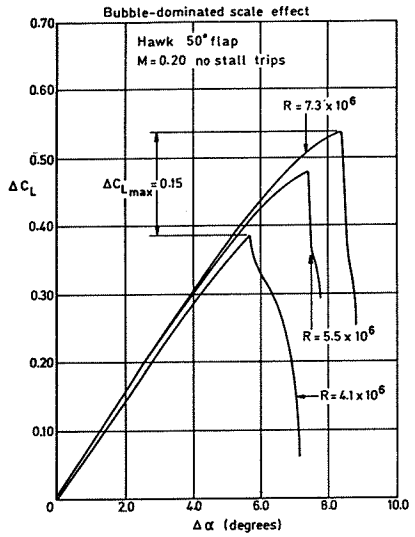

Fig 7 Variation of lift curve with Reynolds number on Hawk model

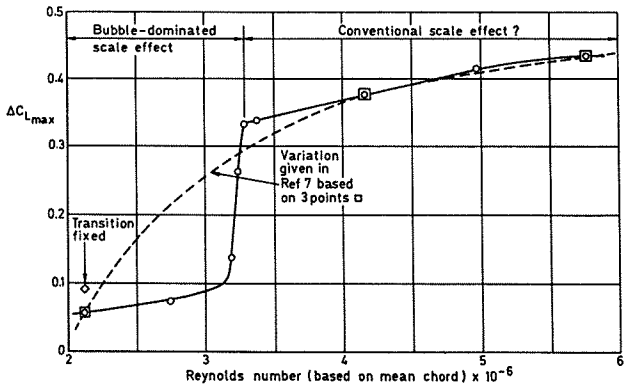

Fig 8 Variation of $C_{L_{max}}$ with Reynolds number on Model 477 25° slat 2% underlap, 20° flap

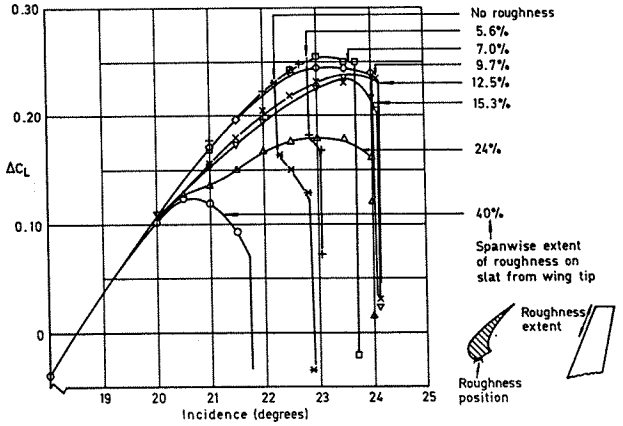

Fig 9 Effect of different spanwise extents of roughness on the stall pattern of Model 477 at R = 2.1 × 10^6

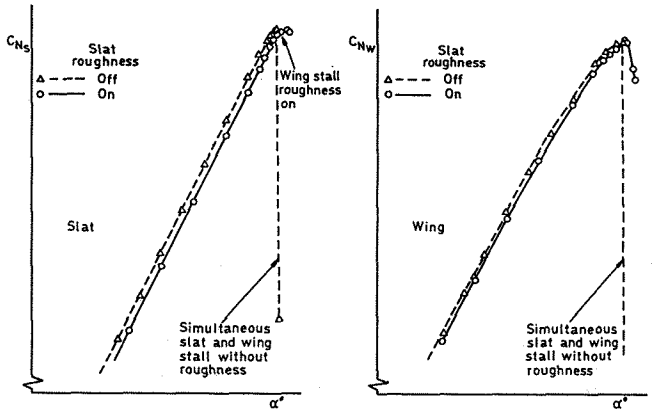

Fig 10 Comparison of sectional normal force curves at an outboard station on main wing and slat of Model 477 with and without slat roughness

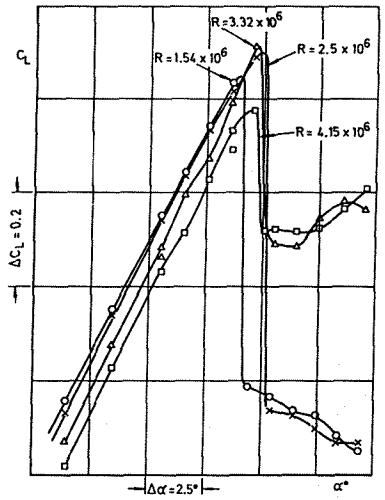

Fig 11 Reynolds number effect on low sweep transport aircraft model with 40° flap

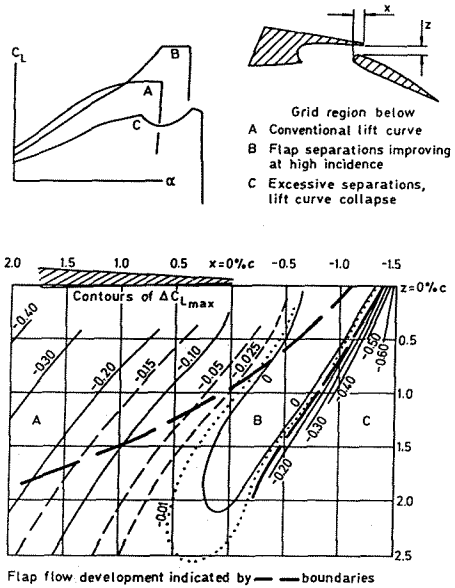

Fig 12 Results from optimisation of a 40° single-slotted flap on a quasi-two-dimensional end-plate model

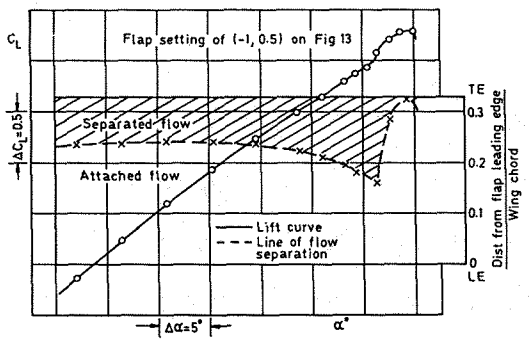

Fig 13 Variation of separation on 40° flap with incidence on a quasi-two-dimensional end-plate model

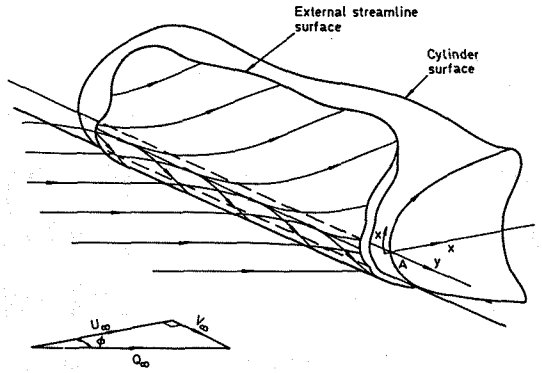

Fig 14 Flow near the leading edge of a swept cylinder (abstracted from Ref 23)

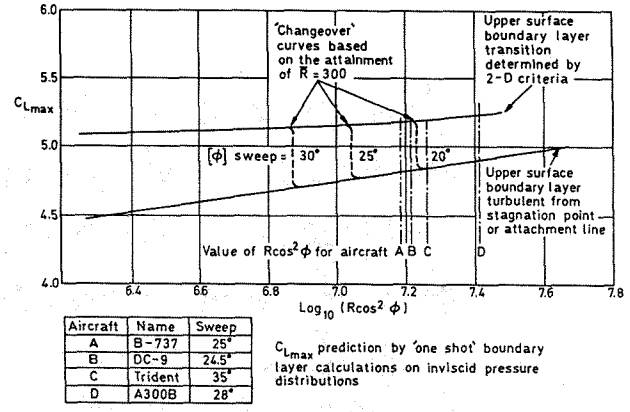

Aircraft	Name	Sweep
A	B-737	25°
B	DC-9	24.5°
C	Trident	35°
D	A300B	28°

$C_{L_{max}}$ prediction by 'one shot' boundary layer calculations on inviscid pressure distributions

Fig 15 Predicted $C_{L_{max}}$ variation with Reynolds number for flexible Krueger leading-edge device

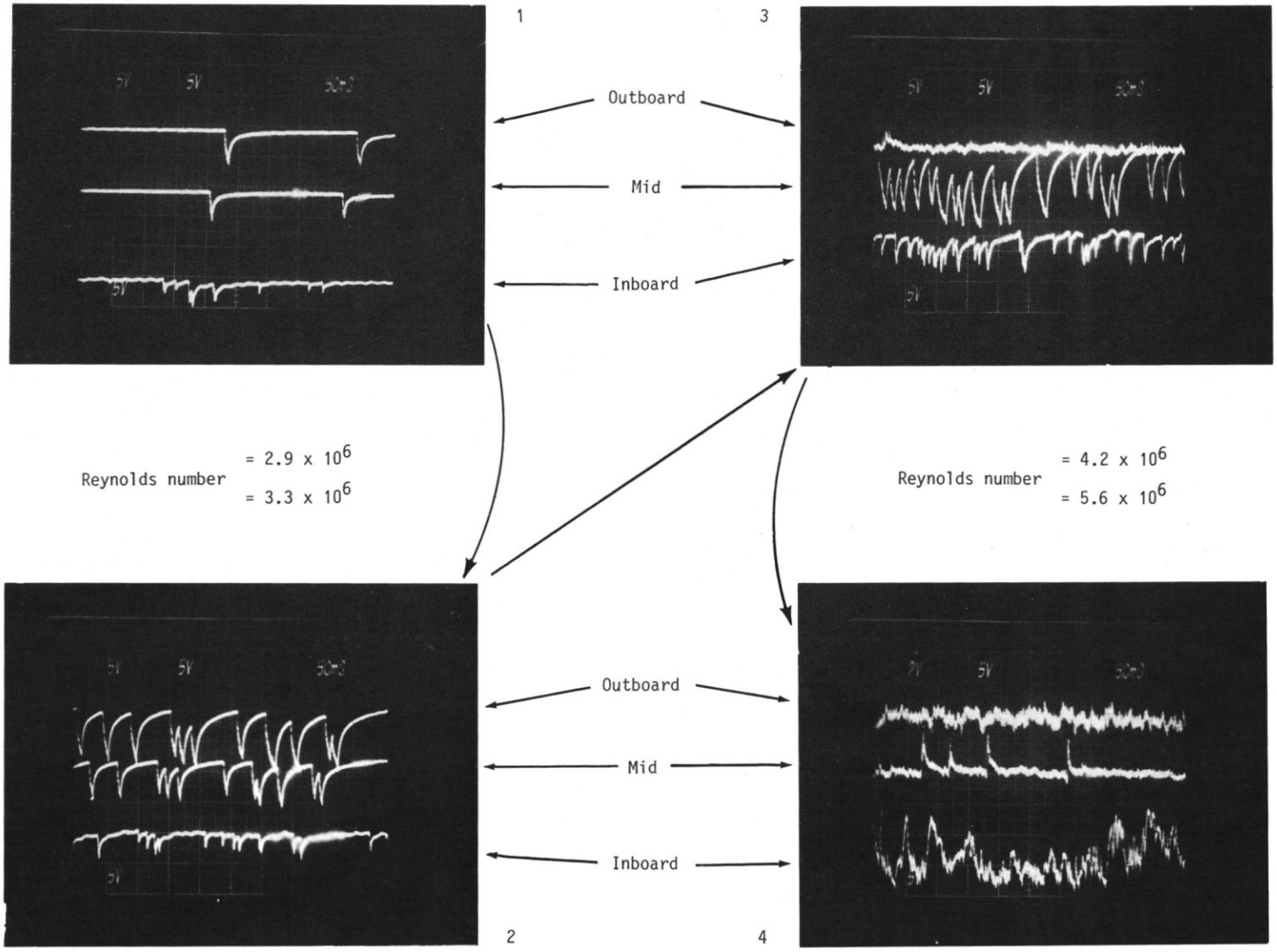

Fig 16 Hot film traces on the attachment line of Model 477 with plain leading-edge. M = 0.16

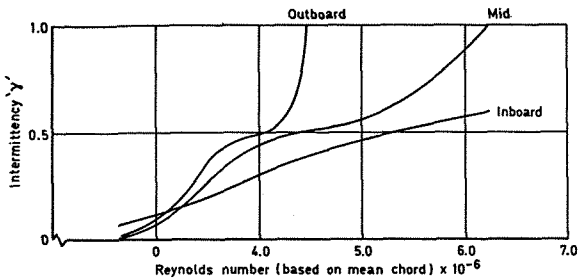

Fig 17 Spanwise variation of attachment line turbulence with Reynolds number - Model 477 plain L/E

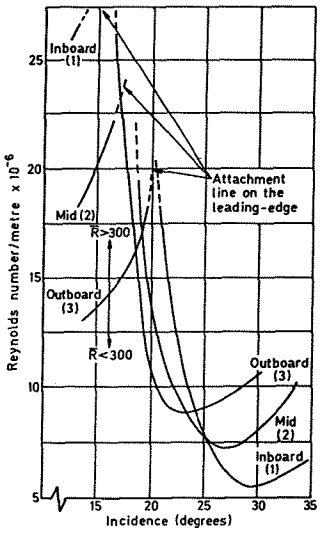

Fig 18 Variation, with incidence, of Reynolds number necessary to achieve $\bar{R}$ = 300 at 3 spanwise stations on Model 495

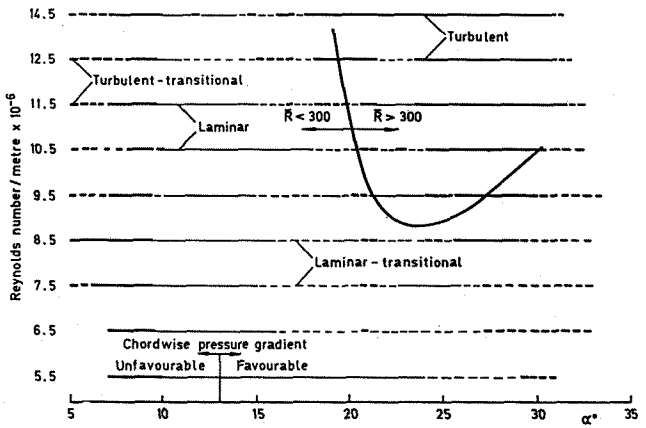

Fig 19 Variation of boundary-layer type with incidence and Reynolds number at an outboard station

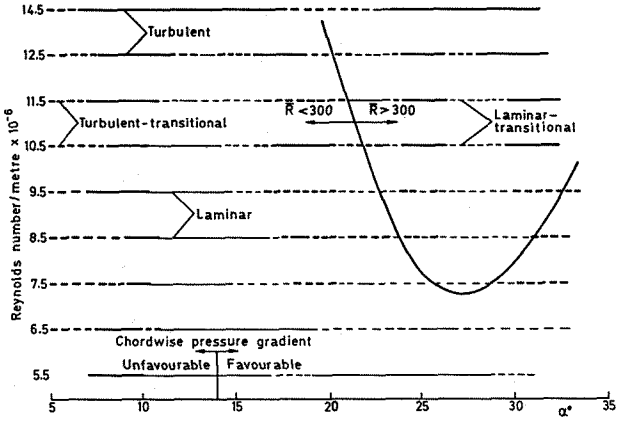

Fig 20 Variation of boundary-layer type with incidence and Reynolds number at a mid station

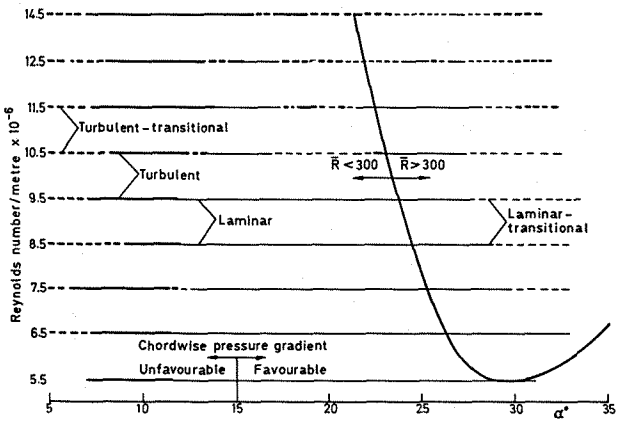

Fig 21 Variation of boundary-layer type with incidence and Reynolds number at an inboard station

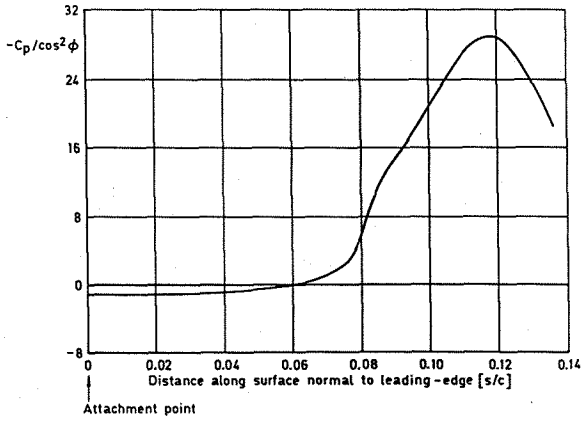

Fig 22 Pressure distribution on M495 at an outboard station near $C_{L_{max}}$

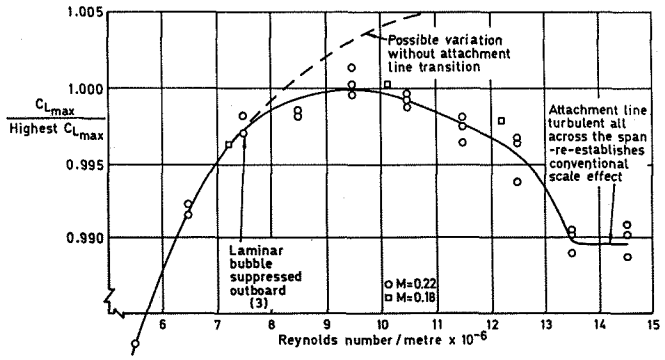

Fig 23 Variation of maximun lift with Reynolds number on Model 495

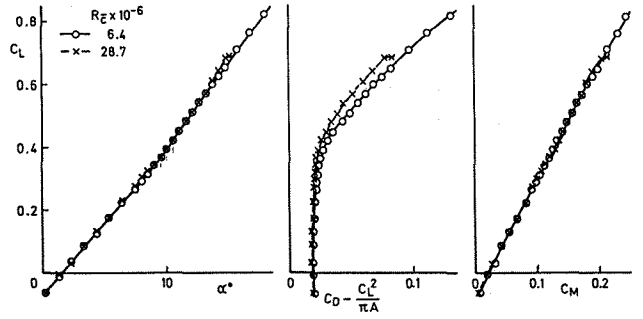

Fig 24 Variation of $C_{L_{max}}$ with Reynolds number on Model 477 with plain leading-edge

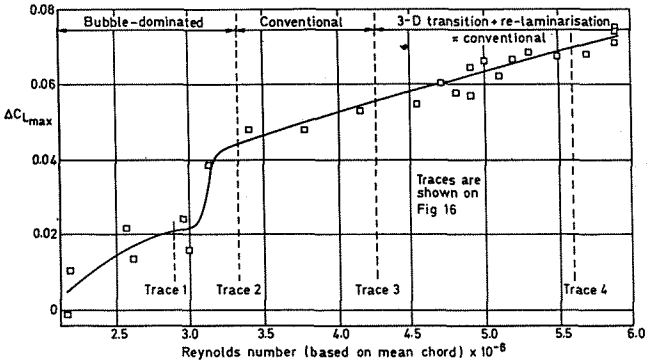

Fig 25 Scale effects on overall forces, M2205, free transition, $M_\infty = 0.6$

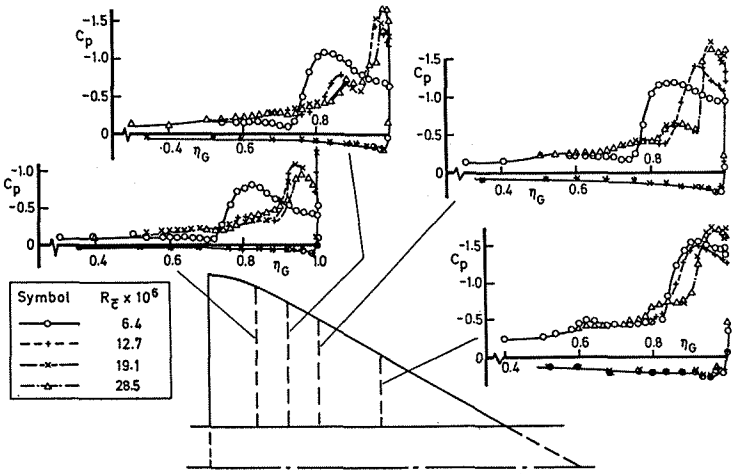

Fig 26 Effect of Reynolds number on pressure distributions, M2205 free transition, $M_\infty = 0.6$, $\alpha = 11.7$, $C_L = 0.48$